







In the format provided by the authors and unedited.

Reduced net methane emissions due to microbial methane oxidation in a warmer Arctic

Youmi Oh ¹, Qianlai Zhuang ^{1,2,3} ✉, Licheng Liu¹, Lisa R. Welp ^{1,2}, Maggie C. Y. Lau^{4,9},
Tullis C. Onstott⁴, David Medvigy ⁵, Lori Bruhwiler⁶, Edward J. Dlugokencky⁶, Gustaf Hugelius ⁷,
Ludovica D'Imperio⁸ and Bo Elberling ⁸

¹Department of Earth, Atmospheric, and Planetary Sciences, Purdue University, West Lafayette, IN, USA. ²Purdue Climate Change Research Center, West Lafayette, IN, USA. ³Department of Agronomy, Purdue University, West Lafayette, IN, USA. ⁴Department of Geosciences, Princeton University, Princeton, NJ, USA. ⁵Department of Biological Sciences, University of Notre Dame, Notre Dame, IN, USA. ⁶NOAA Earth System Research Laboratory, Global Monitoring Division, Boulder, CO, USA. ⁷Department of Physical Geography and Bolin Centre for Climate Research, Stockholm University, Stockholm, Sweden. ⁸Center for Permafrost (CENPERM), University of Copenhagen, Copenhagen, Denmark. ⁹Present address: Laboratory of Extraterrestrial Ocean Systems, Institute of Deep-sea Science and Engineering, Chinese Academy of Sciences, Sanya, China. ✉e-mail: qzhuang@purdue.edu

Supplementary Information for

Reduced net methane emissions due to microbial methane oxidation in a warmer Arctic

Youmi Oh¹, Qianlai Zhuang^{1,2,3*}, Licheng Liu¹, Lisa R. Welp^{1,2}, Maggie C.Y. Lau^{4,9}, Tullis C. Onstott⁴, David Medvigy⁵, Lori Bruhwiler⁶, Edward J. Dlugokencky⁶, Gustaf Hugelius⁷, Ludovica D'Imperio⁸, and Bo Elberling⁸

¹Department of Earth, Atmospheric, and Planetary Sciences, Purdue University, West Lafayette, IN, USA

²Purdue Climate Change Research Center

³Department of Agronomy, Purdue University, West Lafayette, IN, USA

⁴Department of Geosciences, Princeton University, Princeton, NJ, United States

⁵Department of Biological Sciences, University of Notre Dame, Notre Dame, IN, USA

⁶NOAA Earth System Research Laboratory, Global Monitoring Division, Boulder Colorado, USA

⁷Department of Physical Geography and Bolin Centre for Climate Research, Stockholm University, Stockholm 10691, Sweden

⁸Center for Permafrost (CENPERM), University of Copenhagen, DK-1350, Copenhagen, Denmark

⁹Present Address: Laboratory of Extraterrestrial Ocean Systems, Institute of Deep-sea Science and Engineering Chinese Academy of Sciences Sanya China

* Author for correspondence:

Qianlai Zhuang

Tel: +1 (765) 494-9610

Email: qzhuang@purdue.edu

Contents of this file: Supplementary methods 1 to 6, supplementary figures 1 to 16, supplementary tables 1 to 8, and 20 references

1. Comparison of optimized parameters with previous studies

The optimized parameters show maximum potential, temperature and moisture sensitivity of methane production and oxidation in different ecosystems (supplementary tables 3-4 and supplementary figures 2 and 4). In wetlands, the temperature sensitivity of methane emission (P_{CH_4Q10}) ranges 2.5 – 9, corresponding to observations^{1,2}. In boreal wetland ecosystems, methane emission is less sensitive to temperature (low P_{CH_4Q10}), and more oxidation occurs by LAM (high OXI_c), probably due to higher temperature throughout the growing season than in alpine and wet tundra ecosystems. In uplands, the temperature sensitivity (O_{CH_4Q10}) ranged from 1 to 6, also corresponding to observations³. O_{CH_4Q10} was optimized to be lowest for upland wet tundra as our observation data from wet tundra showed consistent methane consumption throughout the growing season⁴ (supplementary figures 1e and 3e). The optimal soil moisture (MV_{opt}) for methane consumption ranges between 0.35 to 0.55 v/v, corresponding to observations⁵. The parameter uncertainty is large for the reference temperature of methane production (T_{PR}) for wetland systems and is large for minimum soil moisture (MV_{min}) for upland systems (supplementary figures 2 and 4).

2. Soil temperature and moisture validation

We validated soil temperature and moisture in the top 10-cm soil depth for alpine tundra, wet tundra, and boreal forest sites where we used the data from the sites for model optimization^{4,6,7}. In general, soil thermal and hydrological modules of TEM simulate Arctic soil temperature and moisture reasonably well (supplementary figure 5). The simulated soil temperature and moisture correspond well with observations, but with a slight under-estimation of temperature and over-estimation of moisture during the growing season.

3. Examples of seasonal changes in $MIC_{biomass}$ in soil columns

Supplementary figure 6 shows an example of seasonal changes in active microbial biomass ($MIC_{biomass}$) in wetland and upland systems at four soil depths. The simulated $MIC_{biomass}$ of MG and HAM are in a reasonable range of previous studies⁸. The seasonal maximum of $MIC_{biomass}$ of MG and HAM are one to two months lagged behind the maximum of soil temperature (supplementary figure 5), which extends the period of methane emission and consumption (Extended Data Figure 1).

In a wetland system, $MIC_{biomass}$ of MG is higher at 50 and 100 cm depths (supplementary figure 6a), where the combined effects of soil temperature, moisture, pH, redox potential, and organic matter

contents are optimal for methanogen (equation (13C)). In an upland system, $MIC_{biomass}$ of HAM is highest at 10 cm depth and is negligible at 50, 100, and 200 cm depths due to the substrate depletion in deeper soils (supplementary figure 6b). The main energy source of HAM – methane and oxygen, mainly comes from the atmosphere, which reduces in concentration with depth as a result of diffusivity. The $MIC_{biomass}$ of HAM at deeper soils are thus negligible because most atmospheric methane is consumed by HAM at top soil layers (equation (13D)).

4. Sensitivity test for XPTEM-XHAM of contemporary period

We varied a transient wetland distribution using satellite-driven Surface Water Microwave Product Series- Global Lakes and Wetlands Database (SWAMPS-GLWD) during 2000-2012 for our sensitivity test⁹. We also conducted 8 sensitivity tests of wetland emission and 6 tests of upland consumption to changes in meteorology and substrate inputs. Specifically, we altered air temperature by $\pm 3^\circ\text{C}$, water table depth by ± 30 cm, and soil moisture, atmospheric methane abundance, permafrost SOC, and NPP by $\pm 30\%$, uniformly for each grid cell, while maintaining all other variables at their default XPTEM-XHAM values.

5. Sensitivity test for XPTEM-XHAM for future projections

We used a static inundation map for our default simulation¹⁰ but applied the transient wetland inundation fraction data by setting the initial inundation fraction same as SWAMPS-GLWD but varying the seasonal and inter-annual fraction of each grid cell using normalized changes in the fraction simulated by the CLM 5.0 SSP3-7 deforestation scenario for a sensitivity test¹¹.

We acknowledge that different model structures and temperature sensitivity among models may cause potential biases in the projected methane emission as temperature increase¹². Thus, we used various Q_{10} of methanogenesis and methanotrophy for our sensitivity test of XPTEM-XHAM for RCP 8.5 scenarios. We referred the temperature sensitivity test of CLM4Me¹³ and varied the Q_{10} of methane production to 2, 3, and 4 with reference temperature of 3°C for low, medium, and high setups, respectively. The Q_{10} of methane oxidation varied to 1, 2, and 3 with reference temperature of 5°C for low, medium, and high setups, respectively, which is smaller than Q_{10} of methane production but still is in a range of observation³. Furthermore, to clarify the effect of projected increase in $[\text{CH}_4]_{\text{atm}}$ from 1.8 to 3.8 ppm for RCP 8.5 scenario (supplementary figures 12), we conducted additional simulation where we keep $[\text{CH}_4]_{\text{atm}}$ to be same as the contemporary level, 1.8 ppm.

6. Importance of Microbial dynamics of LAM

We first need to acknowledge the limitation of observation data to optimize methane processes in wetlands. Most bottom-up methane models, including ours, use observed net wetland methane emissions to optimize methane production by MG and oxidation by LAM where the fraction of each is uncertain¹². Since methane oxidation by LAM is highly dependent on methane emission by MG due to its requirement of high methane concentrations (> 600ppm) for survival and growth¹⁴, we assume that the observed net wetland methane emissions are mainly controlled by microbial dynamics of MG.

However, to clarify the role of LAM in wetland methane emission for both contemporary period and future projection, we ran additional simulations by adding microbial dynamics of LAM into XPTEM-XHAM. In specific, the methane oxidation and microbial biomass changes for LAM were simulated using equations (13B) and (13D) but we set the Michaelis-Menten constant (k_{CH4}) for LAM to be 5 μM (equation (5)), instead of 0.11 μM for HAM (equation (9))¹⁴. For LAM physiology, microbial growth efficiency (ε) of LAM is set to be 0.5, same as HAM, and maintenance energy (m_E) exponentially increases, same as MG and HAM (equation (16))^{15,16}.

The results show that simulations with microbial dynamics of LAM for contemporary period in 2000-2016 are within the uncertainty range of the simulations without LAM microbial dynamics, reflecting the minor role of LAM $MIC_{biomass}$ in current wetland methane emissions (supplementary figures 16a). For with and without physiology simulations of RCP 8.5 scenario, the wetland methane emissions may decrease by $\sim 5 \text{ Tgyr}^{-1}$ by 2100 after LAM microbial dynamics are included, although the difference is within the uncertainty ranges (supplementary figures 16b). Thus, LAM microbial dynamics have a limited contribution to current wetland methane dynamics but may have a potential to decrease wetland emissions due to its increase in $MIC_{biomass}$ in a warmer Arctic.

To better constrain the methane pathways in Arctic wetlands, more observations of subsurface vertical processes using isotopic labeling analysis and inhibitor techniques are necessary¹⁷. The future study shall factor the effects of diverse vertical methane pathways, including LAM microbial dynamics and physiology, when more data are available.

Supplementary figure captions

Supplementary Figure 1. Model-data comparison of methane fluxes for XPTEM-XHAM model. (a-c) wetland methane emission and (d-f) upland methane consumption in $\text{mg m}^{-2} \text{ day}^{-1}$ for (a,d) alpine tundra, (b,e) wet tundra, and (c,f) boreal forest ecosystems.

Supplementary Figure 2. Box plot of normalized optimized parameters for XPTEM-XHAM model.

(a-c) Normalized values of optimized parameters of (1) maximum methane production potential (MGO), (2) Q_{10} temperature sensitivity of methane production ($Q_{CH_4Q_{10}}$), (3) Maximum potential of methane oxidation by LAM (O_{XIC}), and (4) reference temperature for methane production (T_{PR}). (d-f) Normalized values of optimized parameters with 1 standard deviation of (1) maximum potential of methane oxidation by HAM (O_{max}), (2) Q_{10} temperature sensitivity of methane oxidation ($O_{CH_4Q_{10}}$), (3) Maximum soil moisture for methane oxidation (MV_{max}), (4) minimum soil moisture for methane oxidation (MV_{min}) and (5) optimum soil moisture for methane oxidation (MV_{opt}) for (a,d) alpine tundra, (b,e) wet tundra, and (c,f) boreal forests. On each box, the central mark indicates the median, and the bottom and top edges of the box indicate the 25th and 75th percentiles, respectively. The whiskers extend to the most extreme data points not considered outliers, and the outliers are plotted individually using the '+' symbol¹⁸.

Supplementary Figure 3. Model-data comparison of methane fluxes for PTEM-HAM model. (a-c) wetland methane emission and (d-f) upland methane consumption in $\text{mg m}^{-2} \text{ day}^{-1}$ for (a,d) alpine tundra, (b,e) wet tundra, and (c,f) boreal forest ecosystems.

Supplementary Figure 4. Box plot of normalized optimized parameters for PTEM-HAM model.

(a-c) Normalized values of optimized parameters of (1) maximum methane production potential (MGO), (2) Q_{10} temperature sensitivity of methane production ($Q_{CH_4Q_{10}}$), (3) Maximum potential of methane oxidation by LAM (O_{XIC}), and (4) reference temperature for methane production (T_{PR}). (d-f) Normalized values of optimized parameters with 1 standard deviation of (1) maximum potential of methane oxidation by HAM (O_{max}), (2) Q_{10} temperature sensitivity of methane oxidation ($O_{CH_4Q_{10}}$), (3) Maximum soil moisture for methane oxidation (MV_{max}), (4) minimum soil moisture for methane oxidation (MV_{min}) and (5) optimum soil moisture for methane oxidation (MV_{opt}) for (a,d) alpine tundra, (b,e) wet tundra, and (c,f) boreal forests. On each box, the central mark indicates the median, and the bottom and top edges of the box

indicate the 25th and 75th percentiles, respectively. The whiskers extend to the most extreme data points not considered outliers, and the outliers are plotted individually using the '+' symbol¹⁸.

Supplementary Figure 5. Model-data comparison of top soil temperature and moisture. (a,c, and e) daily top 10-cm soil temperature in °C and (b, d, and f) daily top 10-cm volumetric soil moisture in % volume for (a,b) alpine tundra in 2013, (c,d) wet tundra in 2012, and (e,f) boreal forest in 2012.

Supplementary Figure 6. Seasonality of active microbial biomass for four soil depths. Changes in active microbial biomass ($\text{nmol}_{\text{bioC}} \text{L}_{\text{soil}}^{-1}$) of (a) methanogens in wetlands in a boreal forest in 2012¹⁹ and (b) HAM in uplands in a dry tundra in 2013-2015⁶ at 10, 50, 100, and 200 cm soil depths.

Supplementary Figure 7. Inter-annual variability of top soil temperature and moisture. Estimates of pan-arctic (a) annual top 10-cm soil temperature in °C and (b) annual top 10-cm soil moisture in % volume for 2000-2016.

Supplementary Figure 8. Spatial variability of methane fluxes north of 50°N. (a-b) Spatial variability of annual wetland methane emission ($\text{TgCH}_4\text{yr}^{-1}$) averaged over (a) 2000-2016 and (b) RCP 8.5 during 2017-2100 for XPTEM-XHAM model. (c-d) Spatial variability of annual upland methane consumption averaged over (c) 2000-2016 and (d) RCP 8.5 during 2017-2100 north of 50°N for XPTEM-XHAM model. The dotted longitudinal lines are at 30° intervals, and the latitudinal line is at 65°N.

Supplementary Figure 9. Monthly averaged time-varying and static inundated area north of 50°N. Monthly inundated area from time-varying (SWAMPTS-GLWD⁹) and a static estimates (Matthews&Fung, 1987¹⁰) in km^2 from 2000 – 2012.

Supplementary Figure 10. Sensitivity test of methane emission and consumption for XPTEM-XHAM. (a) Changes in pan-arctic wetland methane emission relative to a default simulation after varying temperature, water table, NPP, and permafrost SOC. (b) Changes in pan-arctic upland methane

consumption relative to a default simulation after varying temperature, soil moisture, and atmospheric methane abundance ($[\text{CH}_4]_{\text{atm}}$).

Supplementary Figure 11. Inter-annual variability of methane fluxes during 2017 – 2100. (Left) Annual pan-arctic estimates of (a) wetland methane emission and (b) upland methane consumption for XPTEM-XHAM (blue), PTEM-HAM (yellow), and TEM (red) using RCP 2.6 (dotted), RCP 4.5 (dashed), and RCP 8.5 (solid) north of 50°N. The shaded error bars represent one standard deviation of model results determined by varying the optimized parameters from ensemble simulations. (Right) Mean (symbols) and one standard deviation (bars) in 2100 for each metric.

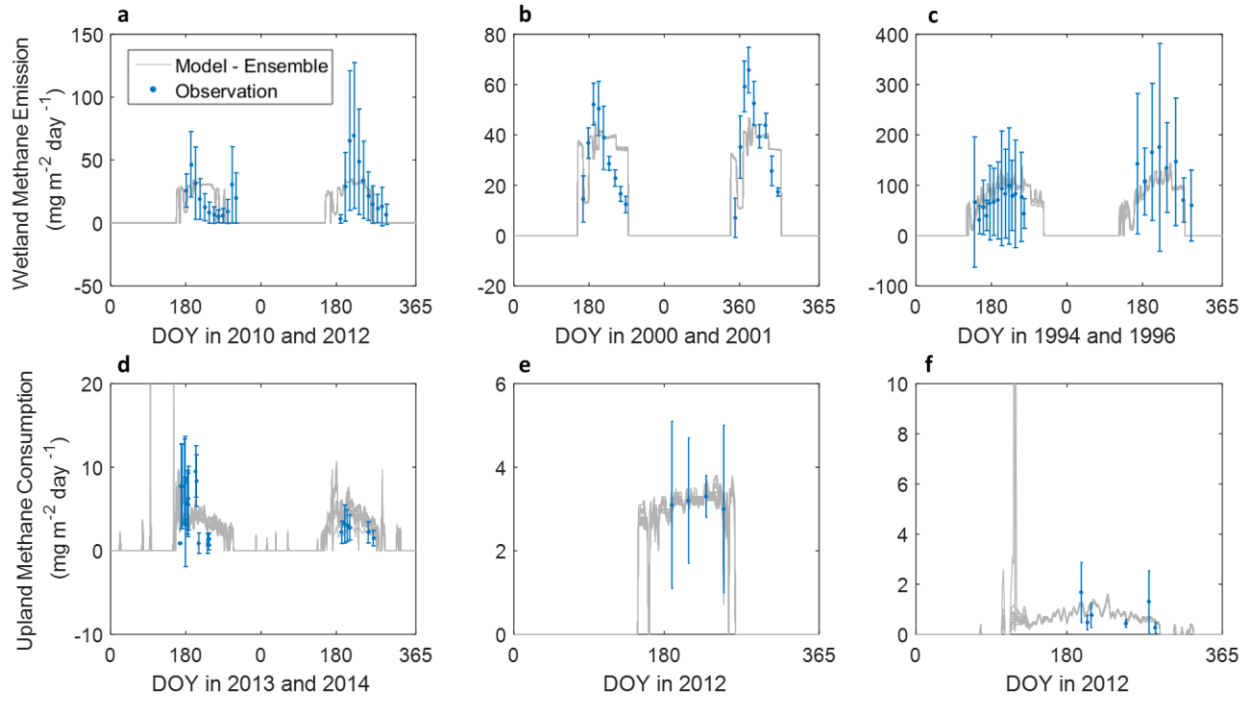
Supplementary Figure 12. Inter-annual variability of soil temperature and moisture and atmospheric methane abundance during 2017 – 2100. Annual averaged estimates of pan-arctic (a) top 10-cm soil temperature in °C, (b) top 10-cm soil moisture in % volume, and (c) atmospheric methane abundance ($[\text{CH}_4]_{\text{air}}$) in ppb using RCP 2.6 (sky blue), RCP 4.5 (green), and RCP 8.5 (dark red) north of 50°N.

Supplementary Figure 13. Spatial variability of top soil temperature and moisture averaged over 2017-2100 for RCP 8.5 north of 50°N. (a) Averaged annual top 10-cm soil temperature in °C and (b) averaged annual top 10-cm soil moisture in % volume. The dotted longitudinal lines are at 30° intervals, and the latitudinal line is at 65°N.

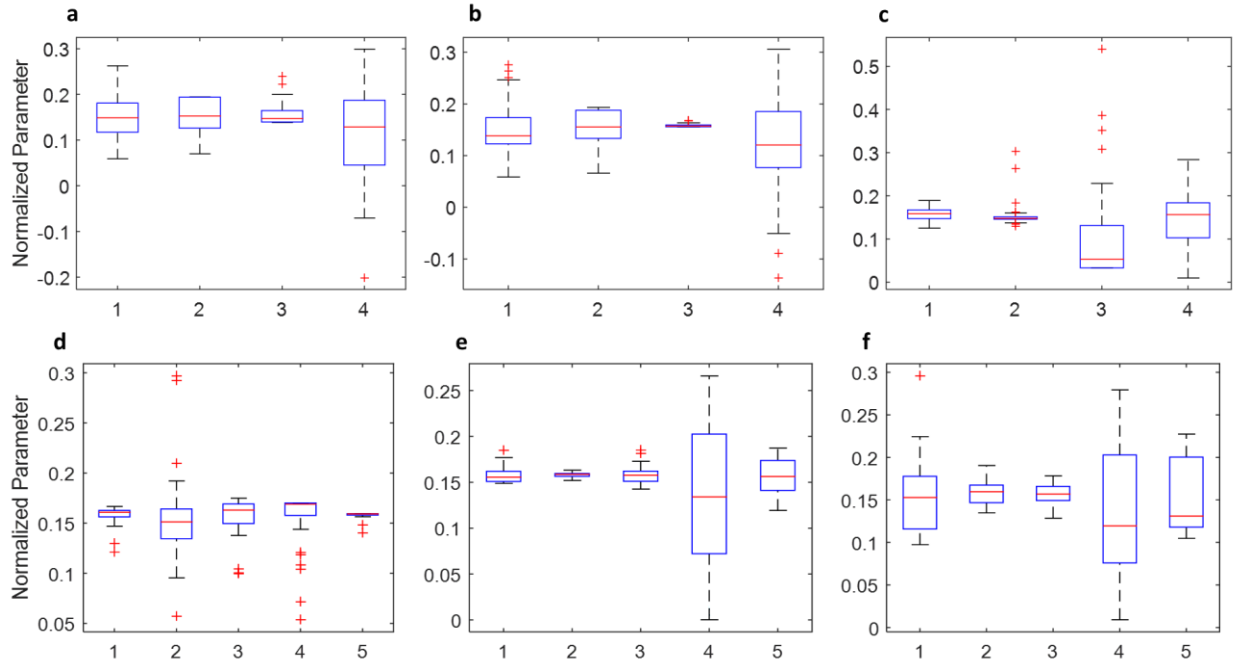
Supplementary Figure 14. Inter-annual variability of methane fluxes for XPTEM-XHAM with its microbial physiology from 2017 – 2100. (Left) Annual estimates of pan-arctic (a) wetland methane emission and (b) upland methane consumption for XPTEM-XHAM without varying m_E (baseline, blue), and XPTEM-XHAM with physiological responses of MG and HAM to temperature change with varying m_E (green) based on RCP 2.6 (dotted), RCP 4.5 (dashed), and RCP 8.5 (solid) north of 50°N. The shaded error bars represent one standard deviation of model results determined by varying the optimized parameters from ensemble simulations. (Right) Mean (symbols) and one standard deviation (bars) in 2100 for each metric.

Supplementary Figure 15. Sensitivity of temperature and atmospheric methane abundance to projections of net methane emission for RCP 8.5 during 2017-2100 north of 50°N. Annual estimates of pan-Arctic net methane emission for XPTEM-XHAM without varying ϵ and m_E (solid blue), XPTEM-XHAM with physiological responses of MG and HAM to temperature change with varying m_E (solid green), and sensitivity tests of the two simulations to Q_{10} changes (dotted, dash-dot, and dashed lines for low, medium, and high Q_{10} setups, respectively) and atmospheric methane abundance to stay at 1.8 ppm (circle marker).

Supplementary Figure 16. Effects of microbial dynamics of LAM to wetland methane emission for contemporary period and RCP 8.5 during 2017-2100 north of 50°N. Annual estimates of pan-Arctic net methane emission for XPTEM-XHAM for (a) contemporary period in 2000-2016 (b) RCP 8.5 scenario in 2017-2100 without varying m_E (blue), XPTEM-XHAM with physiological responses of MG and HAM to temperature change (skyblue), and sensitivity tests of varying microbial dynamics of LAM (red and yellow represent with and without varying m_E , respectively). The shaded error bars represent one standard deviation of model results determined by varying the optimized parameters from ensemble simulations.

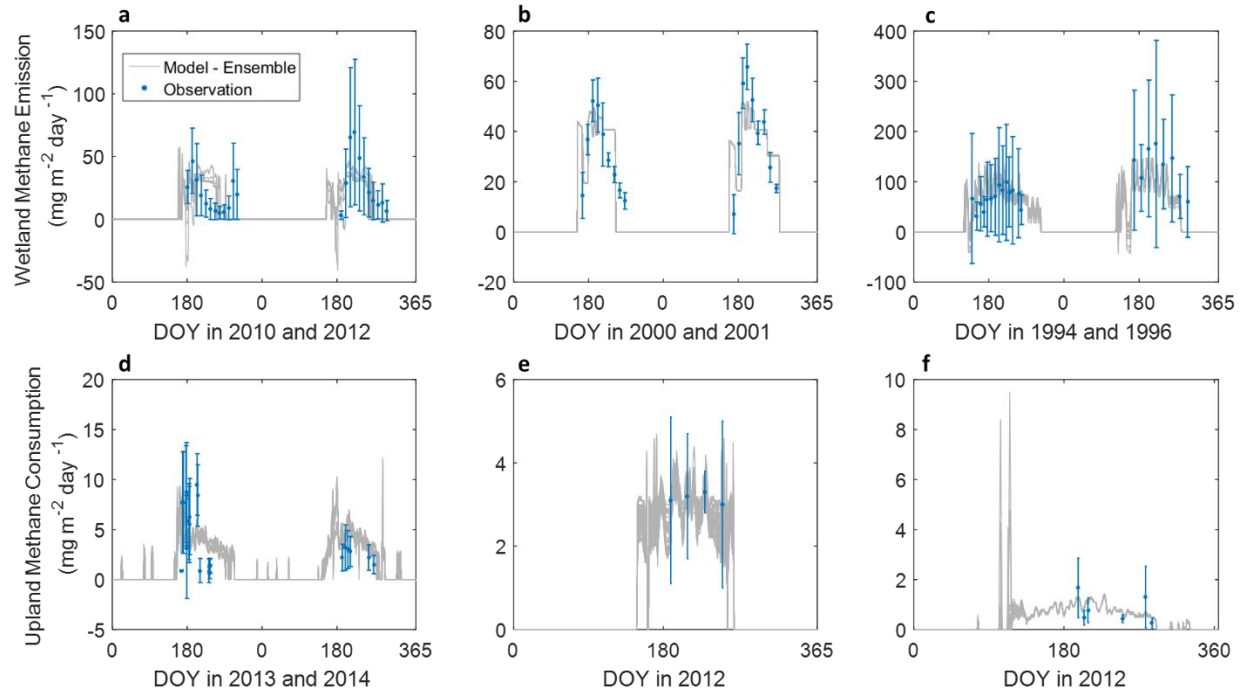


Supplementary Figure 1. Model-data comparison of methane fluxes for XPTEM-XHAM model. (a-c) wetland methane emission and (d-f) upland methane consumption in $\text{mg m}^{-2} \text{day}^{-1}$ for (a,d) alpine tundra, (b,e) wet tundra, and (c,f) boreal forest ecosystems.

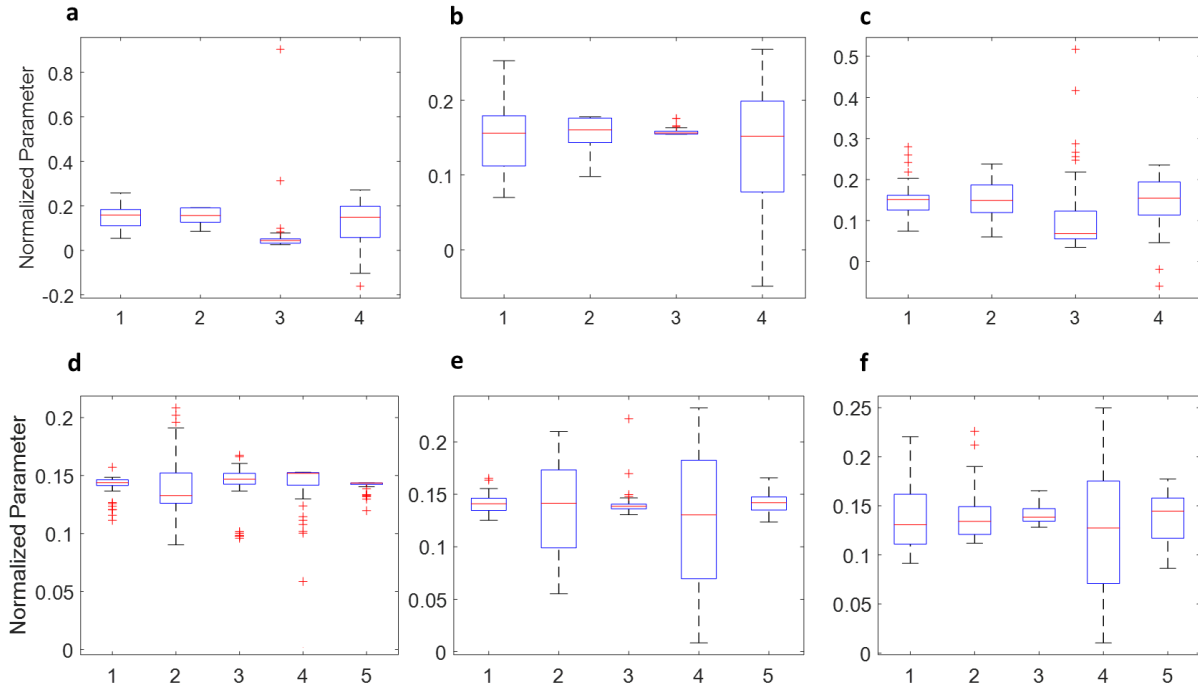


Supplementary Figure 2. Box plot of normalized optimized parameters for XPTEM-XHAM model.

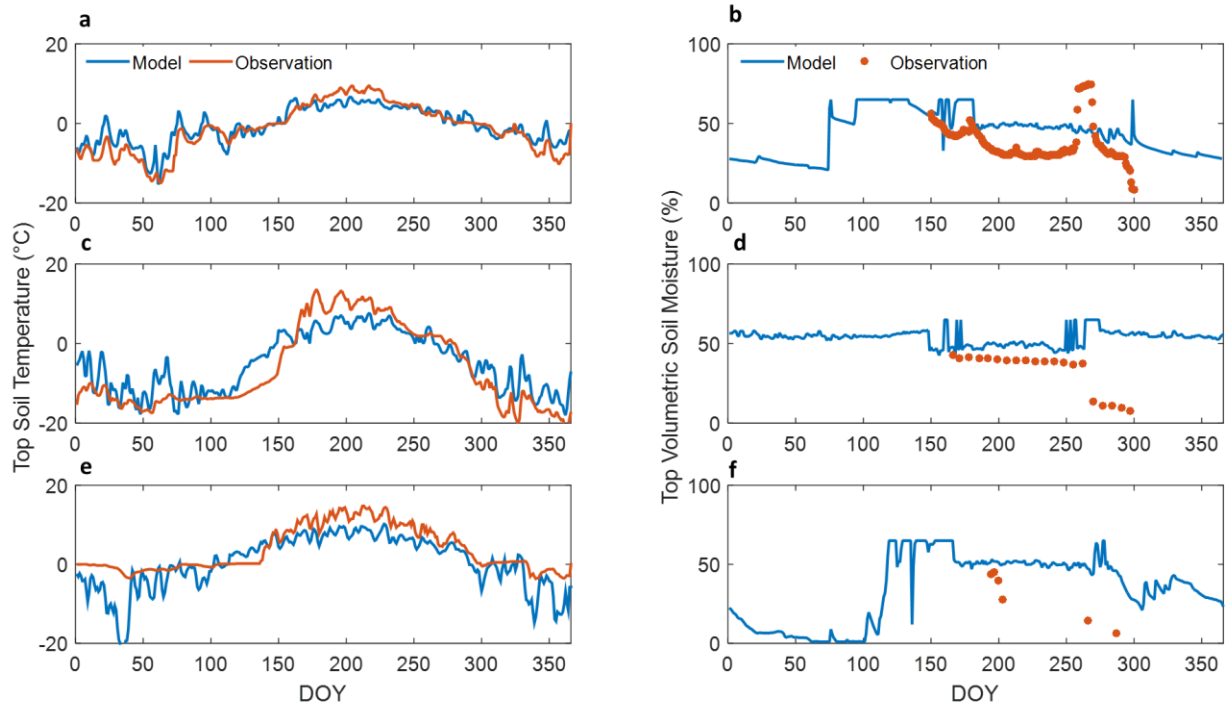
(a-c) Normalized values of optimized parameters of (1) maximum methane production potential (MGO), (2) Q_{10} temperature sensitivity of methane production ($Q_{CH_4Q_{10}}$), (3) Maximum potential of methane oxidation by LAM (O_{XI_C}), and (4) reference temperature for methane production (T_{PR}). (d-f) Normalized values of optimized parameters with 1 standard deviation of (1) maximum potential of methane oxidation by HAM (O_{max}), (2) Q_{10} temperature sensitivity of methane oxidation ($O_{CH_4Q_{10}}$), (3) Maximum soil moisture for methane oxidation (MV_{max}), (4) minimum soil moisture for methane oxidation (MV_{min}) and (5) optimum soil moisture for methane oxidation (MV_{opt}) for (a,d) alpine tundra, (b,e) wet tundra, and (c,f) boreal forests. On each box, the central mark indicates the median, and the bottom and top edges of the box indicate the 25th and 75th percentiles, respectively. The whiskers extend to the most extreme data points not considered outliers, and the outliers are plotted individually using the '+' symbol¹⁸.



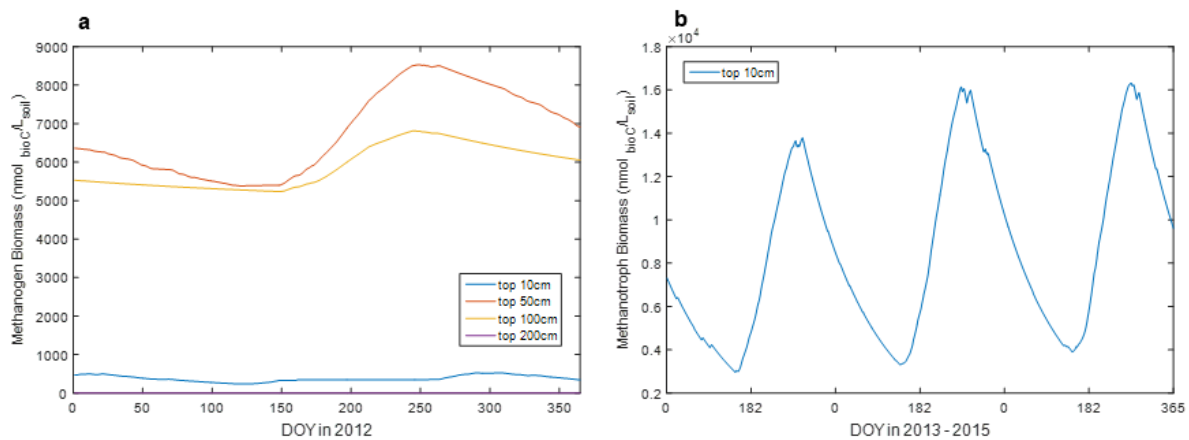
Supplementary Figure 3. Model-data comparison of methane fluxes for PTEM-HAM model. (a-c) wetland methane emission and (d-f) upland methane consumption in $\text{mg m}^{-2} \text{day}^{-1}$ for (a,d) alpine tundra, (b,e) wet tundra, and (c,f) boreal forest ecosystems.



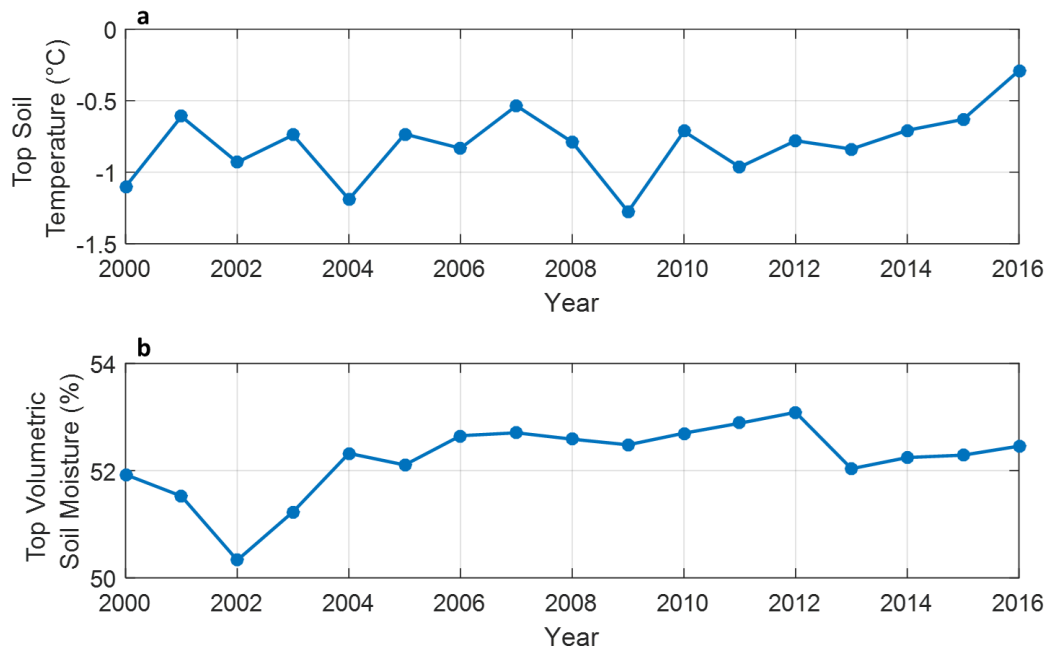
Supplementary Figure 4. Box plot of normalized optimized parameters for PTEM-HAM model. (a-c) Normalized values of optimized parameters of (1) maximum methane production potential (MGO), (2) Q_{10} temperature sensitivity of methane production ($Q_{CH_4Q_{10}}$), (3) Maximum potential of methane oxidation by LAM (O_{XI_C}), and (4) reference temperature for methane production (T_{PR}). (d-f) Normalized values of optimized parameters with 1 standard deviation of (1) maximum potential of methane oxidation by HAM (O_{max}), (2) Q_{10} temperature sensitivity of methane oxidation ($O_{CH_4Q_{10}}$), (3) Maximum soil moisture for methane oxidation (MV_{max}), (4) minimum soil moisture for methane oxidation (MV_{min}) and (5) optimum soil moisture for methane oxidation (MV_{opt}) for (a,d) alpine tundra, (b,e) wet tundra, and (c,f) boreal forests. On each box, the central mark indicates the median, and the bottom and top edges of the box indicate the 25th and 75th percentiles, respectively. The whiskers extend to the most extreme data points not considered outliers, and the outliers are plotted individually using the '+' symbol¹⁸.



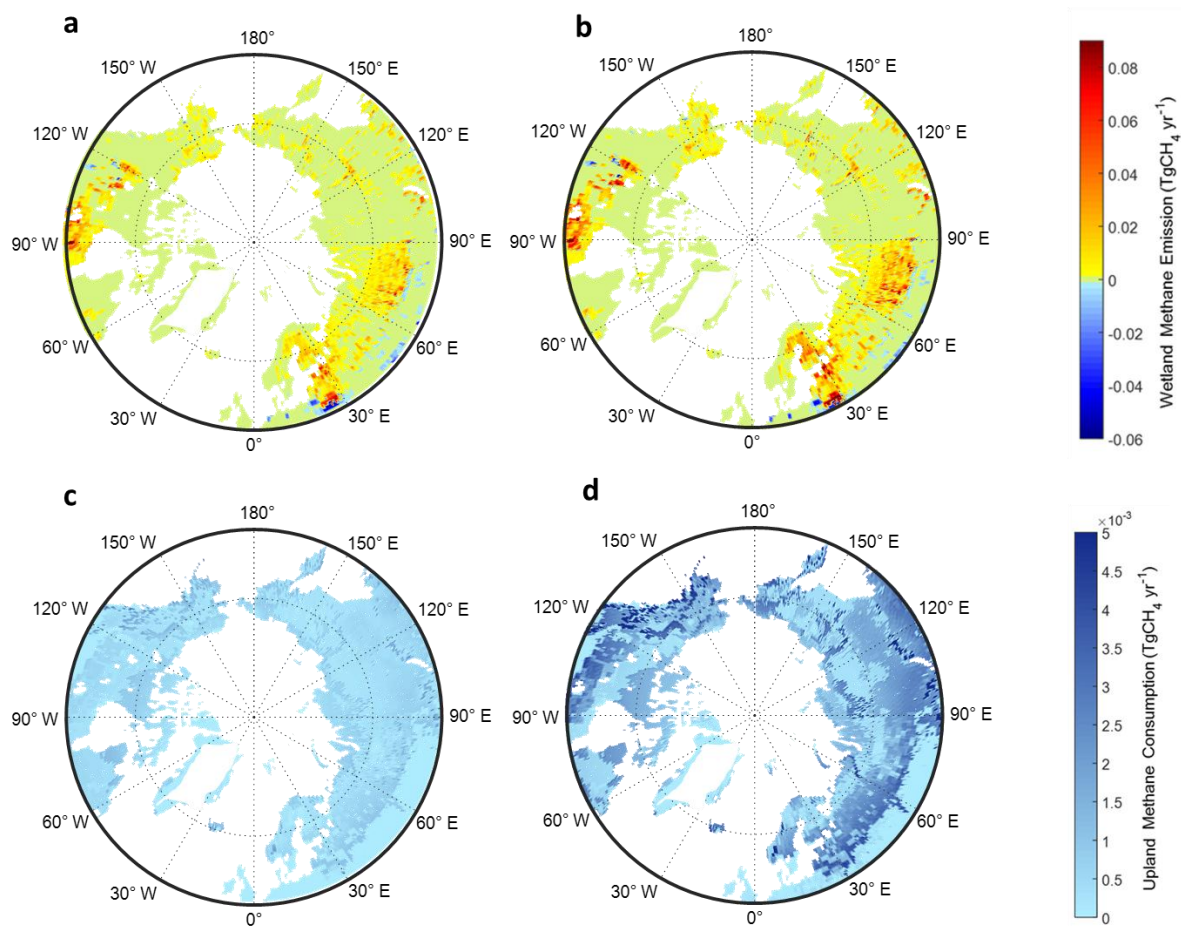
Supplementary Figure 5. Model-data comparison of top soil temperature and moisture. (a,c, and e) daily top 10-cm soil temperature in °C and (b, d, and f) daily top 10-cm volumetric soil moisture in % volume for (a,b) alpine tundra in 2013, (c,d) wet tundra in 2012, and (e,f) boreal forest in 2012.



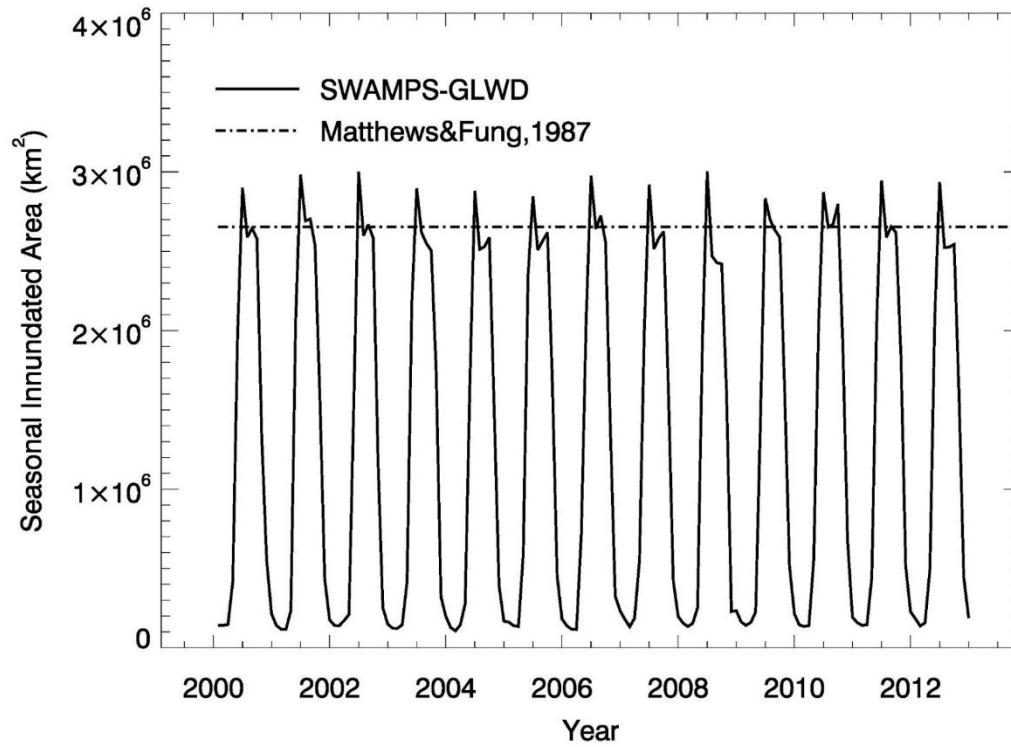
Supplementary Figure 6. Seasonality of active microbial biomass for four soil depths. Changes in active microbial biomass ($\text{nmol}_{\text{bioC}} \text{L}_{\text{soil}}^{-1}$) of (a) methanogens in wetlands in a boreal forest in 2012¹⁹ and (b) HAM in uplands in a dry tundra in 2013-2015⁶ at 10, 50, 100, and 200 cm soil depths.



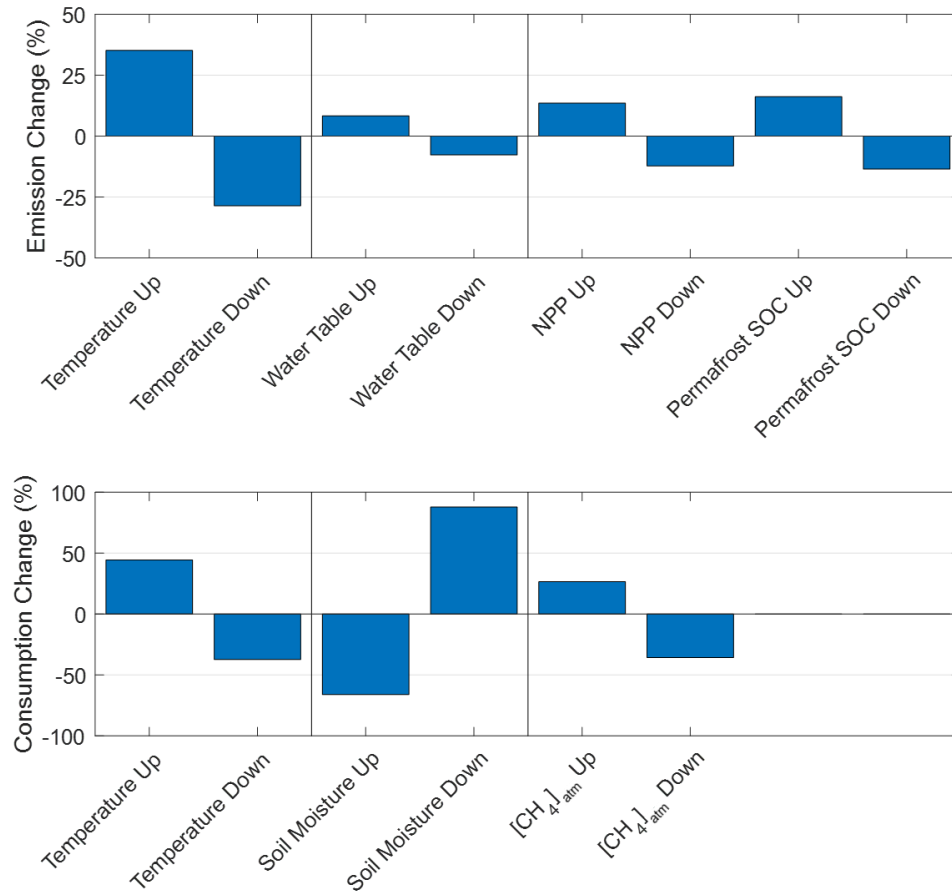
Supplementary Figure 7. Inter-annual variability of top soil temperature and moisture. Estimates of pan-arctic (a) annual top 10-cm soil temperature in °C and (b) annual top 10-cm soil moisture in % volume for 2000-2016.



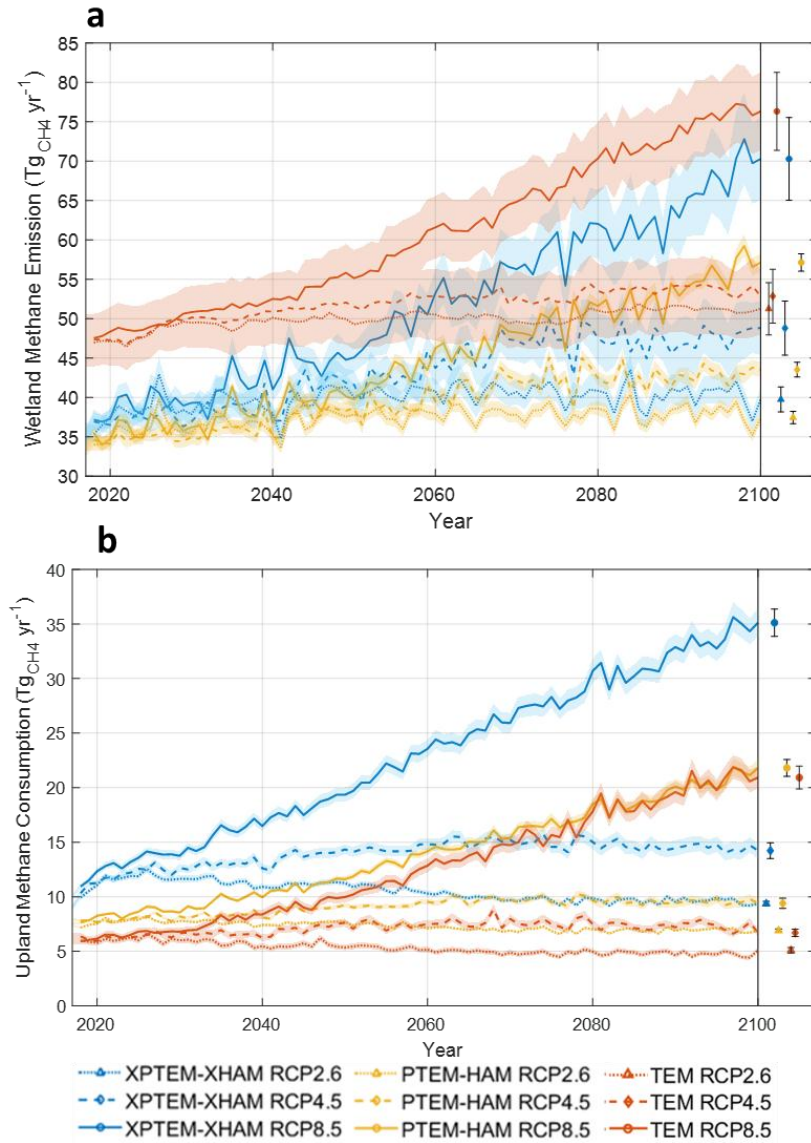
Supplementary Figure 8. Spatial variability of methane fluxes north of 50°N. (a-b) Spatial variability of annual wetland methane emission ($\text{TgCH}_4\text{yr}^{-1}$) averaged over (a) 2000-2016 and (b) RCP 8.5 during 2017-2100 for XPTEM-XHAM model. (c-d) Spatial variability of annual upland methane consumption averaged over (c) 2000-2016 and (d) RCP 8.5 during 2017-2100 north of 50°N for XPTEM-XHAM model. The dotted longitudinal lines are at 30° intervals, and the latitudinal line is at 65°N.



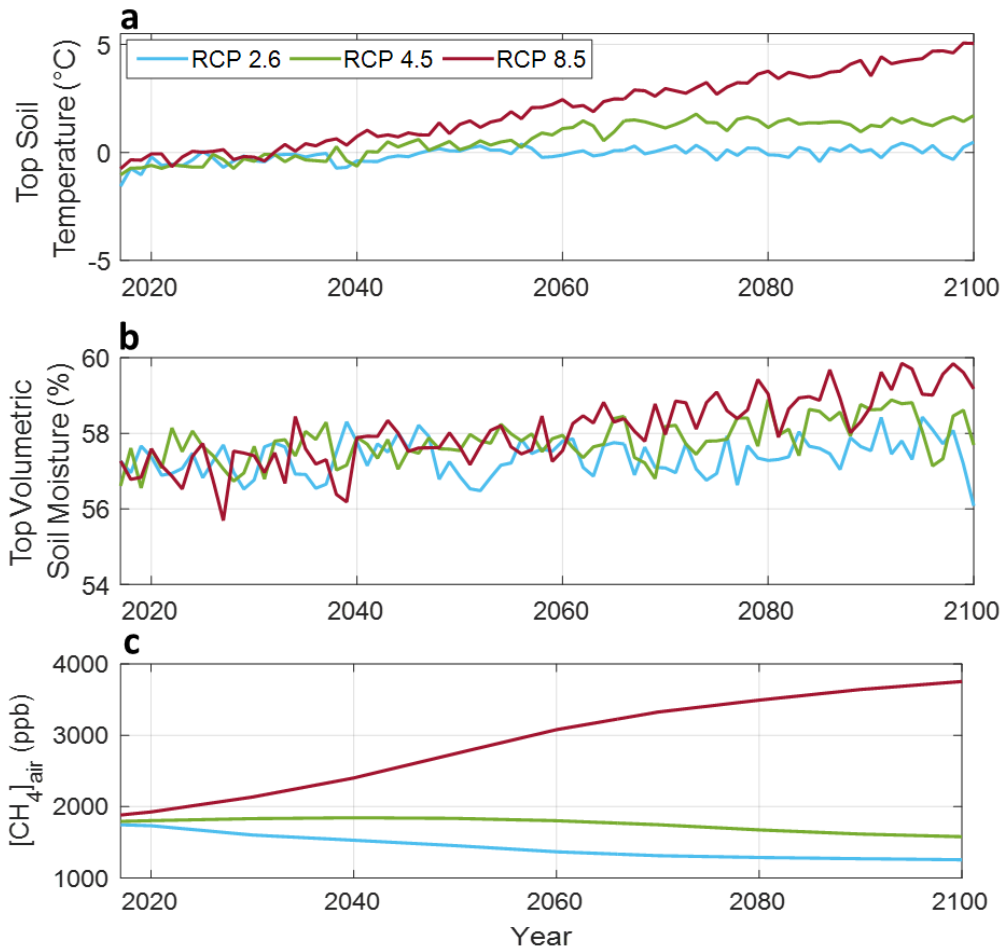
Supplementary Figure 9. Monthly averaged time-varying and static inundated area north of 50°N. Monthly inundated area from time-varying (SWAMPTS-GLWD⁹) and a static estimates (Matthews&Fung, 1987¹⁰) in km² from 2000 – 2012.



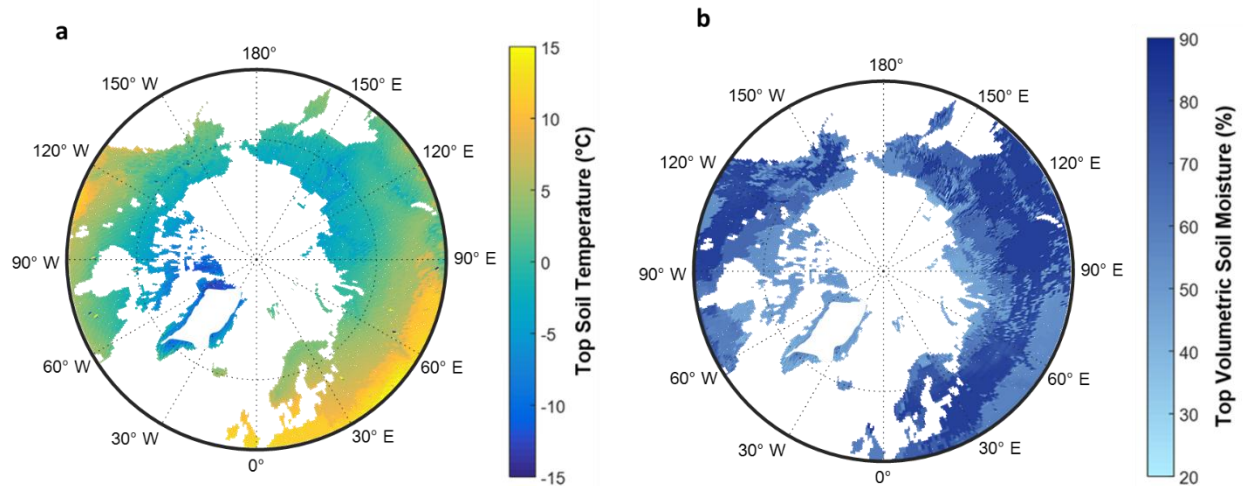
Supplementary Figure 10. Sensitivity test of methane emission and consumption for XPTEM-XHAM. (a) Changes in pan-arctic wetland methane emission relative to a default simulation after varying temperature, water table, NPP, and permafrost SOC. (b) Changes in pan-arctic upland methane consumption relative to a default simulation after varying temperature, soil moisture, and atmospheric methane abundance ($[\text{CH}_4]_{\text{atm}}$).



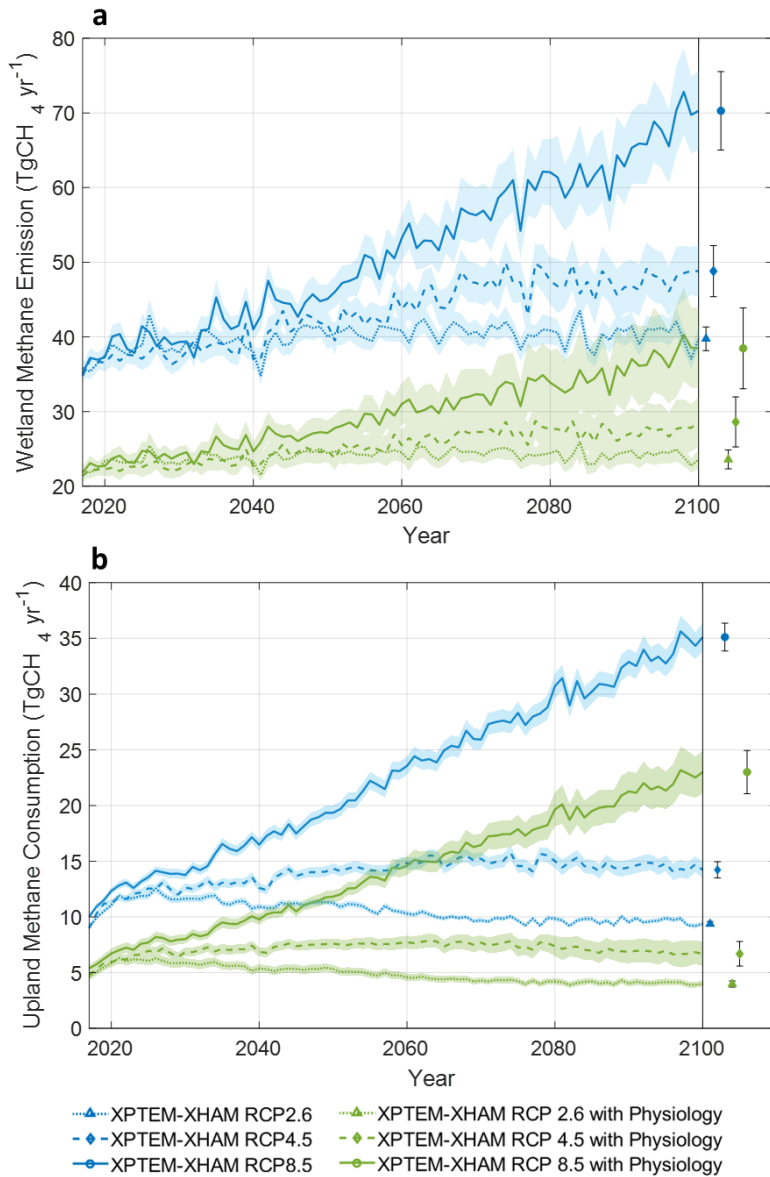
Supplementary Figure 11. Inter-annual variability of methane fluxes during 2017 – 2100. (Left) Annual pan-arctic estimates of (a) wetland methane emission and (b) upland methane consumption for XPTEM-XHAM (blue), PTEM-HAM (yellow), and TEM (red) using RCP 2.6 (dotted), RCP 4.5 (dashed), and RCP 8.5 (solid) north of 50°N . The shaded error bars represent one standard deviation of model results determined by varying the optimized parameters from ensemble simulations. (Right) Mean (symbols) and one standard deviation (bars) in 2100 for each metric.



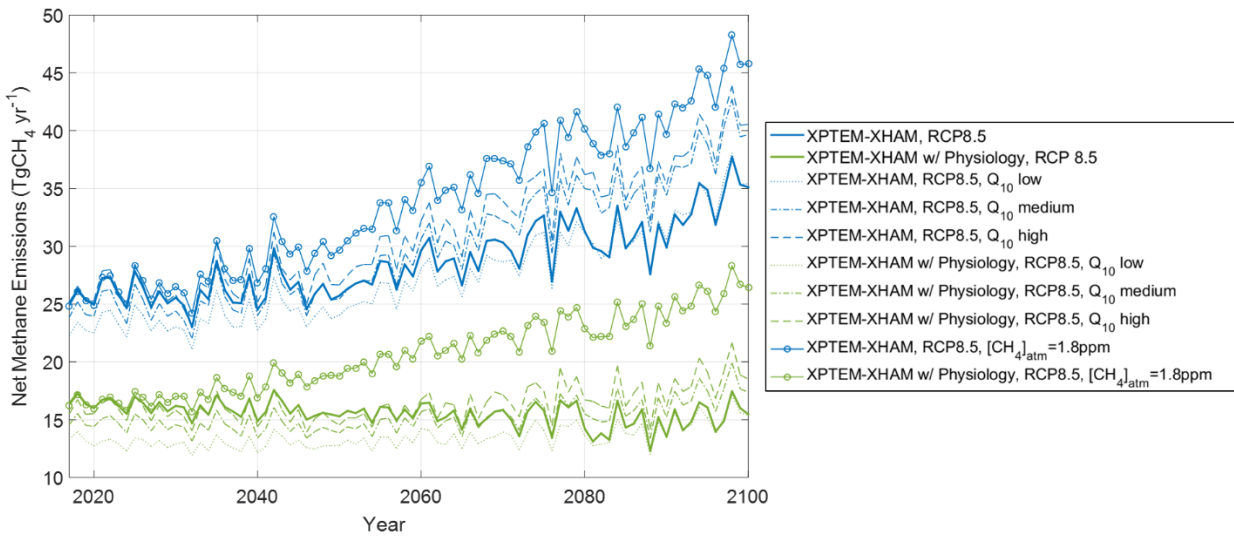
Supplementary Figure 12. Inter-annual variability of soil temperature and moisture and atmospheric methane abundance during 2017 – 2100. Annual averaged estimates of pan-arctic (a) top 10-cm soil temperature in °C, (b) top 10-cm soil moisture in % volume, and (c) atmospheric methane abundance ($[CH_4]_{air}$) in ppb using RCP 2.6 (sky blue), RCP 4.5 (green), and RCP 8.5 (dark red) north of 50°N.



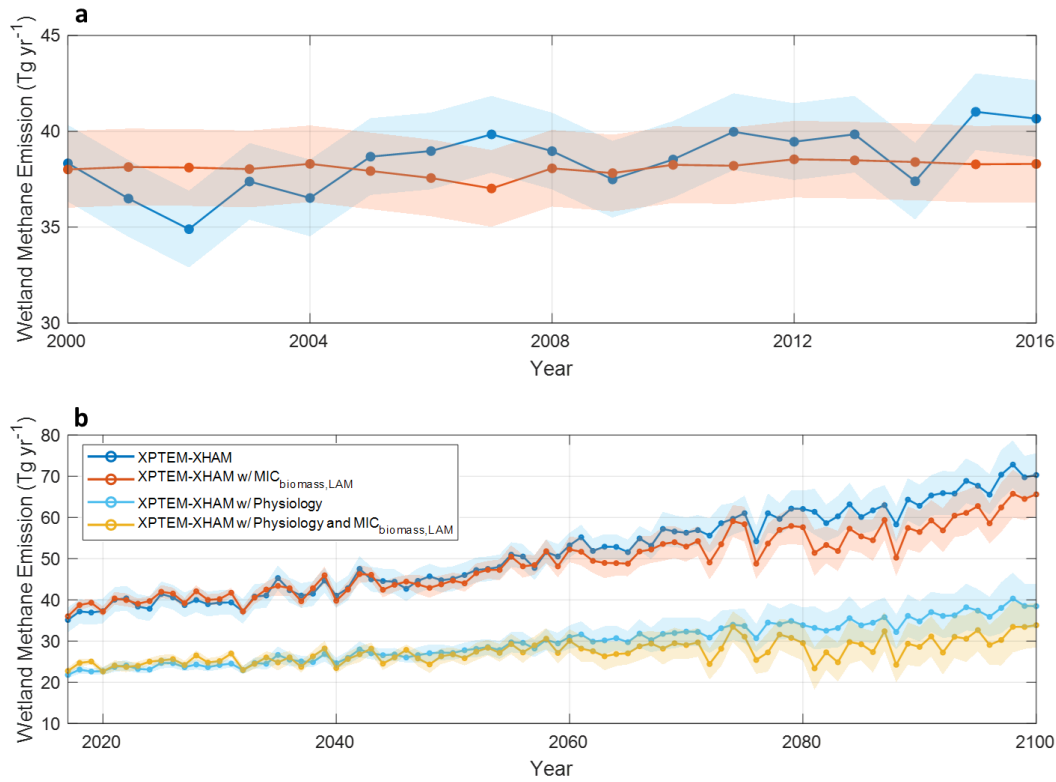
Supplementary Figure 13. Spatial variability of top soil temperature and moisture averaged over 2017-2100 for RCP 8.5 north of 50°N. (a) Averaged annual top 10-cm soil temperature in °C and (b) averaged annual top 10-cm soil moisture in % volume. The dotted longitudinal lines are at 30° intervals, and the latitudinal line is at 65°N.



Supplementary Figure 14. Inter-annual variability of methane fluxes for XPTM-XHAM with its microbial physiology from 2017 – 2100. (Left) Annual estimates of pan-arctic (a) wetland methane emission and (b) upland methane consumption for XPTM-XHAM without varying m_E (baseline, blue), and XPTM-XHAM with physiological responses of MG and HAM to temperature change with varying m_E (green) based on RCP 2.6 (dotted), RCP 4.5 (dashed), and RCP 8.5 (solid) north of 50°N . The shaded error bars represent one standard deviation of model results determined by varying the optimized parameters from ensemble simulations. (Right) Mean (symbols) and one standard deviation (bars) in 2100 for each metric.



Supplementary Figure 15. Sensitivity of temperature and atmospheric methane abundance to projections of net methane emission for RCP 8.5 during 2017-2100 north of 50°N. Annual estimates of pan-Arctic net methane emission for XPTEM-XHAM without varying ϵ and m_E (solid blue), XPTEM-XHAM with physiological responses of MG and HAM to temperature change with varying m_E (solid green), and sensitivity tests of the two simulations to Q_{10} changes (dotted, dash-dot, and dashed lines for low, medium, and high Q_{10} setups, respectively) and atmospheric methane abundance to stay at 1.8 ppm (circle marker).



Supplementary Figure 16. Effects of microbial dynamics of LAM to wetland methane emission for contemporary period and RCP 8.5 during 2017-2100 north of 50°N. Annual estimates of pan-Arctic net methane emission for XPTEM-XHAM for (a) contemporary period in 2000-2016 (b) RCP 8.5 scenario in 2017-2100 without varying m_E (blue), XPTEM-XHAM with physiological responses of MG and HAM to temperature change (skyblue), and sensitivity tests of varying microbial dynamics of LAM (red and yellow represent with and without varying m_E , respectively). The shaded error bars represent one standard deviation of model results determined by varying the optimized parameters from ensemble simulations.

Supplementary table captions

Supplementary Table 1. Information about observation sites for model optimization.

Supplementary Table 2. Variable name, unit, upper and lower boundary of optimized parameters.

Supplementary Table 3. Optimized parameters for PTEM-HAM.

Supplementary Table 4. Optimized parameters for XPTEM-XHAM.

Supplementary Table 5. Summary table of in-situ wetland methane emission and upland methane consumption measured in the Arctic from Emmerton et al. (2014) and Lau et al. (2015).

Supplementary Table 6. Summary table of regional estimation of net methane flux.

Supplementary Table 7. Model-data comparison of regional estimation of net methane flux with one standard deviation ($\text{TgCH}_4\text{yr}^{-1}$).

Supplementary Table 8. Annual mean wetland methane emission, upland methane consumption, and net methane emission ($\text{TgCH}_4\text{yr}^{-1}$) with one standard deviation in 2000 – 2016 for low-Arctic ($50\text{-}65^\circ\text{N}$), high-Arctic ($>65^\circ\text{N}$), and pan-Arctic ($>50^\circ\text{N}$) estimated by TEM, PTEM-HAM, and XPTEM-XHAM.

Supplementary Table 1. Information about observation sites for model optimization.

No.	Vegetation Types	Latitude, Longitude	Meteorological Inputs	Observation Data	References
Uplands					
1	Alpine Desert	70, -53.5	Site observation	CH ₄ flux in 2013-2014	D’Imperio et al., 2016
2	Wet Tundra	74.5, -20.5	Site observation	CH ₄ flux in 2012	Jørgensen et al., 2015
3	Boreal Forest	67.5, 26.5	Site observation	CH ₄ flux in 2012	Dinsmore et al., 2017
Wetlands					
1	Alpine Desert	74.5, -20.5	Site observation	CH ₄ flux in 2010, 2012	<i>Greenland Ecosystem Monitoring Programme</i>
2	Wet Tundra	71, -156.5	CRU	CH ₄ flux in 2000-2001	Harazono et al., 2006
3	Boreal Forest	56, -98.5	Site observation	CH ₄ flux in 2012	Sellers et al., 1997

Supplementary Table 2. Variable name, unit, upper and lower boundary of parameters.

Symbol	Variable name	XPTEM-XHAM			PTEM-HAM		
		Unit	Upper Boundary	Lower Boundary	Unit	Upper Boundary	Lower Boundary
Wetlands							
M_{GO}	Maximum Potential of Methane Production	μM_{SOC} $\mu\text{M}_{\text{bioC}}^{-0.66}$ hr^{-1}	0.05	0.001	$\mu\text{M hr}^{-1}$	5.0	0.1
Q_{CH4Q10}	Q ₁₀ temperature sensitivity	unitless	10.0	1.0	unitless	10.0	1.0
O_{XIc}	Maximum Potential of methane oxidation by LAM	$\mu\text{M hr}^{-1}$	5.0	0.01	$\mu\text{M hr}^{-1}$	5.0	0.01
T_{PR}	Reference temperature for methane production	°C	5.0	-5.0	°C	0.01	-5.0
Uplands							
O_{max}	Maximum Potential of methane oxidation by HAM	μM_{CH4} $\mu\text{M}_{\text{bioC}}^{-0.66}$ hr^{-1}	0.025	0.001	$\mu\text{M hr}^{-1}$	15.0	0.1
O_{CH4Q10}	Q ₁₀ temperature sensitivity	Unitless	10.0	0.5	Unitless	10.0	0.5
MV_{max}	Maximum Volumetric Soil Moisture	v/v	1.0	0.55	v/v	1.0	0.55
MV_{min}	Minimum Volumetric Soil	v/v	0.25	0.0	v/v	0.25	0.0

	Moisture						
MV_{opt}	Optimum Volumetric Soil Moisture	v/v	0.55	0.25	v/v	0.55	0.25

Supplementary Table 3. Optimized parameters for PTEM-HAM.

Wetlands						
No.	Vegetation	M_{GO}	P_{CH4Q10}	O_{XI_C}	T_{PR}	
1	Alpine Desert	0.280±0.094	8.034±1.928	0.028±0.055	2.154±1.908	
2	Wet Tundra	0.415±0.121	8.818±1.179	0.010±0.001	2.438±1.405	
3	Boreal Forest	0.504±0.140	6.296±1.873	0.211±0.194	2.827±1.287	
Uplands						
No.	Vegetation	O_{MAX}	O_{CH4Q10}	M_v_{max}	M_v_{min}	M_v_{opt}
1	Alpine Desert	3.755±0.487	6.240±1.119	0.818±0.818	0.226±0.052	0.541±0.019
2	Wet Tundra	2.422±0.149	2.864±0.925	0.614±0.058	0.134±0.071	0.464±0.032
3	Boreal Forest	0.813±0.188	4.192±0.758	0.853±0.057	0.124±0.067	0.431±0.082

Supplementary Table 4. Optimized parameters for XPTEM-XHAM.

Wetlands						
No.	Vegetation	M_{GO}	P_{CH4Q10}	O_{XIc}	T_{PR}	
1	Alpine Desert	0.016±0.005	7.896±1.971	0.011±0.011	1.750±1.595	
2	Wet Tundra	0.014±0.005	7.985±1.832	0.010±0.0002	1.920±1.529	
3	Boreal Forest	0.015±0.001	2.392±0.484	0.033±0.035	2.490±1.032	
Uplands						
No.	Vegetation	O_{MAX}	O_{CH4Q10}	M_v_{max}	M_v_{min}	M_v_{opt}
1	Alpine Desert	0.0034±0.0002	6.1449±1.1366	0.8090±0.1806	0.1854±0.0814	0.5259±0.0311
2	Wet Tundra	0.0024±0.0002	1.1762±0.1237	0.7947±0.0939	0.1349±0.0688	0.4404±0.0814
3	Boreal Forest	0.0022±0.0005	3.7315±0.3722	0.8553±0.0613	0.1130±0.0682	0.3603±0.0811

Supplementary Table 5. Summary table of in-situ wetland methane emission and upland methane consumption measured in the Arctic from Emmerton et al. (2014)²⁰ and Lau et al. (2015)³.

Wetlands						
No	Location	Latitude (°)	Longitude (°)	Emission Flux (mg m⁻² day⁻¹)	Standard Deviation (mg m⁻² day⁻¹)	References
1	James Bay, CA	51.3	-80.3	34.0	18.0	Roulet et al., 1994, Moore et al., 1994
2	Hudson Bay lowlands, CA	53.0	-90.0	40.8	16.3	Picket-Heaps 2011
3	Schefferville, CA	54.5	-66.5	30.0	12.0	Bubier, 1995, Adamsen and King, 1993
4	Churchill, CA	58.5	-94.1	54.0	21.6	Roulet et al., 1994, Moore et al., 1994
5	Bethel, US	60.5	-161.5	58.0	28.0	Bartlett et al., 1992, Fan et al., 1992
6	Daring Lake, CA	64.5	-111.4	62.0	24.8	Wilson and Humphreys, 2012
7	Vorkuta, RU	67.2	63.4	44.0	39.0	Berestovakaya et al., 2005, Heikkinen et al., 2002a
8	Yamal, RU	68.1	71.4	58.0	23.2	Eheyer et al., 2002
9	Stordalen, SE	68.2	19.0	58.0	32.0	Oquist and Svensson, 2002
10	Toolik, US	68.4	-149.4	41.5	36.5	King et al., 1998
11	Flakkerhuk, Disko Island, GL	69.0	-53.0	1.6	1.0	Johansen et al., 2011
12	Kaamanen, FI	69.1	27.2	48.5	20.0	Corradi et al., 2005
13	Cherskii, RU	69.4	161.2	223.0	58.0	Nakano et al., 2000
14	Indigirka, RU	70.5	147.3	83.0	20.0	Parmentier et al., 2011

15	Barrow, US	71.2	-156.4	37.0	7.3	Lara et al., 2012, Sturtevant et al., 2012
16	Tiski, RU	71.3	130.0	23.0	9.2	Nakano et al., 2000
17	Lena Delta, RU	72.2	126.3	20.5	10.5	Sachs et al., 2008
18	Northern RU	72.5	141.5	39.1	39.0	Christensen et al., 1995
19	Zackenberg Valley, GL	74.2	-21.0	26.5	5.5	Mastepanov 2008, Christensen 2000
20	Zackenberg, GL	74.3	-20.3	103.0	35.5	Strom et al., 2012
21	Alexandra Fjord, Ellesmere Island, CA	78.5	-75.6	1.5	6.4	Brummell et al., 2012
22	Ny-Ålesund, Svalbard	79.0	12.0	45.5	0.6	Adachi et al., 2006
23	Northern RU	72.5	141.5	39.0	39.0	Sachs et al., 2008
24	Alaska, US	69.0	-152.5	27.0	20.0	Morrissey and Livingston, 1992
25	Ellesmere I., CA	82.0	-71.2	0.7	0.5	Emmertson et al., 2014
26	Saskatchewan, CA	53.8	-104.6	189.2	34.7	Sellers et al., 1997
27	Manitoba, CA	55.9	-98.4	94.1	89.9	Seller et al., 1997
28	Poikovsky Bog, RU	56.9	82.9	173.9	157.7	Glagolev et al., 2011
29	Poikovsky Mire, RU	56.9	82.9	195.2	180.7	Glagolev et al., 2011
30	Khanty- Mansijsk, RU	60.9	68.7	78.6	47.1	Glagolev et al., 2011

Uplands						
No	Location	Latitude	Longitude	Consumption Flux (mg m⁻² day⁻¹)	Standard Deviation (mg m⁻² day⁻¹)	References
1	Moscow, Puschino	54.5	37.37	0.31	0.1	Kizilova et al., 2013
2	Lipetsk, Danki	54.0	37.31	0.48	0.18	Kizilova et al., 2013
3	Schefferville, CA	54.5	-66.5	3.0	1.2	Bubier, 1995
4	Bonanza Creek, Alaska, US	64.5	-148.2	0.2	0.2	Whalen et al., 1992
5	Stordalen, SE	68.2	19.0	3.0	2.0	Jackowicz-Korczynski et al., 2010
6	Flakkerhuk, Disko Island, GL	69.0	-53.0	0.6	0.5	Johansen et al., 2011
7	Lena River Delta, RU	72.2	126.3	1.7	0.7	Liebner et al., 2011
8	Zackenbergl Valley, GL	74.2	-21.0	0.02	0.01	Christensen 2000, Christensen 2012
9	Zackenbergl, GL	74.3	-20.3	0.3	0.1	Ström et al., 2012
10	Okse Bay, Ellesmere Island, CA	77.8	-87.4	0.9	0.8	Brummell et al., 2014
11	Alexandra Fjord, Ellesmere Island, CA	78.5	-75.5	4.5	2.0	Brummell et al., 2012
12	Ny-Ålesund, Svalbard	79.0	12.0	2.4	1.7	Adachi et al., 2006
13	Expedition	79.2	-90.5	0.2	0.0	Allan 2014,

	Fjord, Axel Heiberg Island, CA					Stackhouse 2016, Lau 2016
14	Patterson River, Ellesmere Island, CA	82.4	-63.5	0.2	0.0	Brummell et al., 2014
15	Ellesmere I., CA	80.0	-69.0	0.6	0.2	Lamb et al., 2011, Stewart et al., 2012
16	Ellesmere I., CA	82.0	-71.2	1.4	0.6	Emmerton et al., 2014

Supplementary Table 6. Summary table of observed regional estimation of net methane flux.

Region	Latitude	Longitude	Net methane flux (TgCH₄yr⁻¹)	Methods	References
Upland					
NE Greenland	74 to 81	-30 to -15	1.3×10^{-3}	Field Study	Jørgensen et al., 2015
W Greenland	69 to 70	-52 to -55	15×10^{-9}	Field Study	D'Imperio et al., 2016
Wetland					
Hudson Bay Lowland	47 to 60	-100 to -80	3.5 – 6.5	Field Study and Inversion	Bloom et al., 2010
West Siberia	54 to 70	65 to 85	4.8 – 7.2	Field Study and Inversion	Bohn et al., 2015
Alaska	50 to 75	-160 to -120	1.48 – 2.0	Field Study and Inversion	Miller et al., 2016

Supplementary Table 7. Model-data comparison of regional estimation of net methane flux with one standard deviation ($\text{TgCH}_4\text{yr}^{-1}$).

		Observation	XPTM-XHAM	PTEM-HAM	TEM
Upland					
1	NE Greenland	1.3×10^{-3}	1.0×10^{-3}	1.1×10^{-3}	0.2×10^{-3}
2	W Greenland	15×10^{-9}	13.5×10^{-9}	7.5×10^{-9}	7.5×10^{-9}
Wetland					
3	Hudson Bay Lowland	3.5 – 6.5	4.72 ± 0.21	3.97 ± 0.22	4.23 ± 0.20
4	West Siberia	4.8 – 7.2	6.69 ± 0.34	7.46 ± 0.22	8.03 ± 0.25
5	Alaska	1.48 – 2.0	0.88 ± 0.06	1.18 ± 0.03	0.66 ± 0.02

Supplementary Table 8. Annual mean wetland methane emission, upland methane consumption, and net methane emission (TgCH₄yr⁻¹) with one standard deviation in 2000 – 2016 for low-Arctic (50-65 °N), high-Arctic (>65°N), and pan-Arctic (>50°N) estimated by TEM, PTEM-HAM, and XPTEM-XHAM.

		Emission (TgCH₄yr⁻¹)	Consumption (TgCH₄yr⁻¹)	Net Emission (TgCH₄yr⁻¹)
TEM	Low-Arctic	37.70 ± 1.99	3.12 ± 0.16	34.58 ± 1.99
	High-Arctic	3.73 ± 0.60	1.04 ± 0.05	2.69 ± 0.60
	Pan-Arctic	41.43 ± 2.59	4.16 ± 0.21	37.27 ± 2.59
PTEM-HAM	Low-Arctic	26.83 ± 2.08	3.83 ± 0.23	23.00 ± 2.08
	High-Arctic	6.76 ± 1.05	2.32 ± 0.15	4.44 ± 1.05
	Pan-Arctic	33.59 ± 3.13	6.15 ± 0.38	27.44 ± 3.13
XPTEM- XHAM	Low-Arctic	32.60 ± 2.03	6.19 ± 0.34	26.41 ± 2.03
	High-Arctic	6.22 ± 1.00	3.33 ± 0.25	2.89 ± 1.00
	Pan-Arctic	38.82 ± 3.03	9.52 ± 0.59	29.30 ± 3.03

References

1. Segers, R. Methane production and methane consumption: A review of processes underlying wetland methane fluxes. *Biogeochemistry* **41**, 23–51 (1998).
2. Roy Chowdhury, T. *et al.* Stoichiometry and temperature sensitivity of methanogenesis and CO₂ production from saturated polygonal tundra in Barrow, Alaska. *Glob. Chang. Biol.* **21**, 722–737 (2015).
3. Lau, M. C. Y. *et al.* An active atmospheric methane sink in high Arctic mineral cryosols. *ISME J.* **9**, 1880–1891 (2015).
4. Juncher Jørgensen, C., Lund Johansen, K. M., Westergaard-Nielsen, A. & Elberling, B. Net regional methane sink in High Arctic soils of northeast Greenland. *Nat. Geosci.* **8**, 20–23 (2015).
5. Whalen, S. C. & Reeburgh, W. S. Moisture and temperature sensitivity of CH₄ oxidation in boreal soils. *Soil Biol. Biochem.* **28**, 1271–1281 (1996).
6. D’Imperio, L., Nielsen, C. S., Westergaard-Nielsen, A., Michelsen, A. & Elberling, B. Methane oxidation in contrasting soil types: responses to experimental warming with implication for landscape-integrated CH₄ budget. *Glob. Chang. Biol.* **23**, 966–976 (2017).
7. Dinsmore, K. J. *et al.* Growing season CH₄ and N₂O fluxes from a subarctic landscape in northern Finland; From chamber to landscape scale. *Biogeosciences* **14**, 799–815 (2017).
8. Conrad, R. Microbial Ecology of Methanogens and Methanotrophs. *Adv. Agron.* **96**, 1–63 (2007).
9. Poulter, B. *et al.* Global wetland contribution to 2000 – 2012 atmospheric methane growth rate dynamics. *Environ. Res. Lett.* **12**, (2017).
10. Matthews, Elaine, and Fung, I. Methane emission from natural wetlands: Global distribution, area, and environmental characteristics of sources. *Global Biogeochem. Cycles* **1**, 61–86 (1987).
11. Lawrence, D. *et al.* Technical Description of version 5.0 of the Community Land Model (CLM). *Natl. Cent. Atmos. Res. (NCAR), NCAR Tech. Note NCAR/TN-478+ STR* **257**, (2018).
12. Xu, X. *et al.* Reviews and syntheses: Four decades of modeling methane cycling in terrestrial ecosystems. *Biogeosciences* **13**, 3735–3755 (2016).
13. Riley, W. J. *et al.* Barriers to predicting changes in global terrestrial methane fluxes: Analyses using CLM4Me, a methane biogeochemistry model integrated in CESM. *Biogeosciences* **8**, 1925–1953 (2011).

14. Baani, M. & Liesack, W. Two isozymes of particulate methane monooxygenase with different methane oxidation kinetics are found in *Methylocystis* sp. strain SC2. *Proc. Natl. Acad. Sci. U. S. A.* **105**, 10203–10208 (2008).
15. Trimmer, M. *et al.* Riverbed methanotrophy sustained by high carbon conversion efficiency. *ISME J.* **9**, 2304–2314 (2015).
16. Tijhuis, L., Van Loosdrecht, M. C. M. & Heijnen, J. J. A thermodynamically based correlation for maintenance gibbs energy requirements in aerobic and anaerobic chemotrophic growth. *Biotechnol. Bioeng.* **42**, 509–519 (1993).
17. Pedersen, E. P., Michelsen, A. & Elberling, B. In situ CH₄ oxidation inhibition and ¹³CH₄ labeling reveal methane oxidation and emission patterns in a subarctic heath ecosystem. *Biogeochemistry* **138**, 197–213 (2018).
18. Higham, D. J. & Higham, N. J. *MATLAB guide*. vol. 150 (Siam, 2016).
19. Sellers, P. J. *et al.* BOREAS in 1997: Experiment overview, scientific results, and future directions. *J. Geophys. Res. Atmos.* **102**, 28731–28769 (1997).
20. Emmerton, C. A. *et al.* The net exchange of methane with high Arctic landscapes during the summer growing season. *Biogeosciences* **11**, 3095–3106 (2014).